Hydrometallurgy 213 (2022) 105916

Contents lists available at ScienceDirect

Hydrometallurgy

journal homepage: www.elsevier.com/locate/hydromet

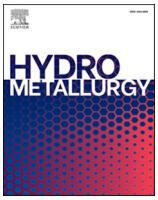

Recovery of scandium from acidic waste solutions by means of polymer inclusion membranes

Sebastian Hedwig [a,b], Manuel Kraus [b], Meret Amrein [a], Johannes Stiehm [c], Edwin C. Constable [b], Markus Lenz [a,d,*]

[a] FHNW, Institute for Ecopreneurship, Hofackerstrasse 30, 4132 Muttenz, Switzerland
[b] University of Basel, Department of Chemistry, Mattenstrasse 24a, 4058 Basel, Switzerland
[c] Bielefeld University, Department of Chemistry, Universitätsstr. 25, 33619 Bielefeld, Germany
[d] Wageningen University, Sub-Department of Environmental Technology, Bornse Weilanden 9, 6700 AA, Wageningen, the Netherlands

ARTICLE INFO

Keywords:
Resource recovery
Critical raw material
Membrane filtration
TiO_2 chloride route
Waste valorisation

ABSTRACT

Scandium is a raw material with properties that promise considerable potential for application in alloys to enable aviation fuel savings and as dopants for use in sustainable energy production using solid oxide fuel cells. Despite these attractive properties, scandium is rarely used due to its scarcity and unreliable supply. Therefore, new strategies for scandium recovery are of economic priority. In this study, polymer inclusion membranes (PIMs) consisting of PVDF-HFP, 2-NPOE and DEHPA, were optimised for selective scandium separation from real TiO_2 production waste. With the optimised system, >60% of the scandium was recovered with high selectivity, resulting in scandium mole fraction at more than two orders of magnitude higher in the receiving phase than in the original waste. This suggests PIMs may be an effective way to recover scandium from bulk waste, thus easing the scarcity and insecurity that currently limit its bulk application.

1. Introduction

In recent decades, many nations have been highly dependent on the import of raw materials, thus creating uncertainty in terms of supply security and price stability (Fröhlich et al., 2017). Consequently, a 'raw materials initiative' was launched by the European Union in 2008 to define measures to secure a sustainable and affordable raw material supply for the future (European Commission, 2017, 2020). One raw material that is considered particularly critical to the EU economy is the rare earth metal scandium (Sc) (European Commission, 2017, 2020). Currently, Sc has two major potential applications: as an alloying metal for aluminium (Al) and as an essential component in solid oxide fuel cells (SOFCs). In aluminium alloys, Sc shows the highest reinforcement increase per atomic percent, making it the most efficient known additive in this regard (Ahmad, 2003). In addition, Sc—Al alloys show improved corrosion resistance, fatigue behaviour and weldability. Specialised aerospace alloys such as Scalmalloy®, requiring just ~0.2% (*w*/w) of Sc, offer weight savings of up to 20% in aircraft (Remmen et al., 2019). To date, the majority of Sc (90% of annual global production) is used for scandia-stabilised zirconia, a solid electrolyte for SOFCs. This ceramic material exhibits considerably enhanced conductivity and lower operating temperatures than alternatives such as yttrium-stabilised zirconia (Binnemans et al., 2018; Spivey et al., 2011). Thus, the use of Sc can effectively lower operation costs and boost energy conversion efficiency.

Despite high demand, global Sc supply is relatively low (~15–25 t $year^{-1}$ in 2021), resulting in high prices (~US$4,370,000 t^{-1}; Table S1) (Gambogi, 2022; Shanghai Metals Market, 2022). The average Sc concentration in the Earth's crust is estimated to be 22 ppm (25 g/t), which is comparable to cobalt (25 ppm) (Lide, 2004; Sykes et al., 2016). However, there are no high-concentration primary sources for Sc due to lack of selective affinity for common ore-forming anions. Hence, Sc is found in low concentrations in over 100 minerals and is won only as a by-product of mining other elements (U.S. Geological Survey, 2020). Only very rarely have primary Sc deposits above 100 ppm been reported (Reid et al., 2017).

Industrial waste, in particular from the production of white pigment (TiO_2), has been identified as a major secondary source of Sc, due to its ready availability, high volume and (relatively) high Sc concentration (Vind et al., 2018; Wang et al., 2011). The major processes for TiO_2 production, namely the sulfate route and chloride route, account for an

* Corresponding author at: FHNW, Institute for Ecopreneurship, Hofackerstrasse 30, 4132 Muttenz, Switzerland.
E-mail address: markus.lenz@fhnw.ch (M. Lenz).

https://doi.org/10.1016/j.hydromet.2022.105916
Received 3 August 2021; Received in revised form 2 June 2022; Accepted 5 June 2022
Available online 9 June 2022

annual global production of ~3.7 Mt. and 3.3 Mt., respectively (Perks and Mudd, 2019). The chloride route is claimed to be superior in terms of energy demand, labour-intensity and waste generation (Gázquez et al., 2014; Perks and Mudd, 2019). For this, high-grade TiO_2 (>85%) ores are converted into volatile $TiCl_4$ by reaction with coke and elemental chlorine at high temperature (900–1000 °C). After purification by fractional distillation of the $TiCl_4$ and reaction with oxygen, pure TiO_2 pigment is obtained (Gázquez et al., 2014). A hydrochloric acid solution is generated as waste during such production. This contains unreacted ore, coke and dissolved metal chlorides and may have major elements such as Ti, Fe and Al and also traces of naturally occurring radionuclides and rare earth elements (Perks and Mudd, 2019; Remmen et al., 2019). The Sc concentration in this acidic waste can be as high as 76–90 ppm, which is considerably higher than for bauxite leachates (Förstner et al., 1995; Remmen et al., 2019; Vind et al., 2018; Wang et al., 2011). Currently, Sc is lost after neutralisation of the waste and deposition of a hydroxide cake. The production of one ton of TiO_2 generates approximately 0.2 t of filter cake (Förstner et al., 1995). Annually, the chloride route generates and disposes of ~0.7 Mt. of dry waste containing up to 220 t of Sc (Hoffmann et al., 2019). To date, few routes for Sc recovery from TiO_2 waste have been investigated (Feuling, 1989; Hartley et al., 2014; Remmen et al., 2019; Wang et al., 2011). Recently, membrane-based processes using either nanofiltration (Remmen et al., 2019) or polymer inclusion membranes (PIMs) have been proposed (Sharaf et al., 2018; Yoshida et al., 2019a; Yoshida et al., 2019b).

Compared to conventional separation technologies such as distillation or solvent extraction (SX), membrane processes offer considerably lower energy and material/chemical consumption (Almeida et al., 2012; Remmen et al., 2019; Sholl and Lively, 2016). The role of membrane processes is becoming increasingly important, as they can reduce the energy consumption of large-scale industrial separation processes by up to 90% (Sholl and Lively, 2016). The key to success for a given application is finding suitable membranes that provide high separation selectivity and high throughput/production rates, and there is steadily growing interest in the research and development of new and improved membranes. The PIMs comprise a class of membranes that allow for the selective extraction and transport of a target solute, such as metal ions, from a feed to a receiving phase. In principle, PIMs are dense, hydrophobic thin films that incorporate lipophilic ligands as extraction agents ('carriers'). When brought into contact with an aqueous solution containing metal ions (the feed phase), the carriers may complex these ions and extract them into the membrane phase. Subsequently, the PIM can release the extracted ions by exposure to an aqueous solution (receiving phase) capable of cleaving the previously formed carrier complexes, for example by protonation. These steps are similar to extraction and stripping in SX (Cortina and Aguilar Sanjuán, 2008) or adsorption and elution using solvent impregnated resins (Batra et al., 2022). In contrast to these conventional approaches, the two-dimensional shape of the PIMs allows single-stage uptake and release of metals. Therefore, the membrane is placed between the feed and the receiving phase. Metals can then be complexed and taken up on the feed side, diffused through the PIM and released on the opposite side, regenerating the carrier. Thus, transmembrane metal transport is achieved (Fig. S1) (Nghiem et al., 2006).

The development of PIMs can benefit from the knowledge gained on SX, especially concerning the efficiency and selectivity of organic extraction agents towards certain elements (Wang and Cheng, 2011).

Recently, Sharaf et al. reported the use of cellulose triacetate–based PIMs for the separation of Sc from five competing lanthanides in nitric acid media at pH 4 (Sharaf et al., 2018). The PIMs contained a mixture of mono-2-ethylhexyl (2-ethylhexyl)phosphonate (PC-88A) and decanoic acid as carriers. After optimisation of membrane composition and the receiving phase, they achieved 96.7% Sc transport across the membrane within 96 h of operation. Remarkably, almost no co-transport of competing metals in the model feed was observed (Sharaf et al., 2018). Yoshida et al. (2019a, 2019b) reported amic acids as carriers for Sc transport across PIMs (Yoshida et al., 2019a; Yoshida et al., 2019b) and demonstrated excellent selectivity for Sc with respect to 11 different metals (including Y, Dy, Cr and Al), with only Fe(III) being co-transported. After 96 h, 94% Sc was recovered from sulfuric acid (pH 3), with only minor transport of competing metals, except for Fe(III), which was transported with 32% efficiency (Yoshida et al., 2019a; Yoshida et al., 2019b).

Despite these promising approaches, all PIM studies to date have used artificial model solutions to study Sc recovery. These may have been over-simplified by using equimolar element concentrations, too high dilutions, or solutions in which only a limited number of elements were present and which did not model real waste compositions (Remmen et al., 2019) in which Sc is present only in minute concentrations (mg L^{-1}) in a cocktail of major impurities (multiple g L^{-1}). In this study, PIMs were assessed for Sc extraction from real TiO_2 acid wastes. The PIM composition was first systematically optimised for efficiency, speed and selectivity of Sc extraction using a design of experiment (DoE) approach (Antony, 2014; Dean et al., 2017). After identification of the most efficient receiving phase in extraction/elution experiments, the optimised PIMs were tested in transport experiments, including elevated temperature tests.

2. Materials and methods

2.1. Chemicals and solutions

Unless otherwise stated, all chemicals and solvents were purchased from Sigma-Aldrich (Switzerland) and used without further purification.

All aqueous solutions were prepared using ultrapure water (<18 MΩ; Barnstead Smart2Pure water purification system, ThermoFisher Scientific, Switzerland). Poly(vinylidene fluoride-*co*-hexafluoropropylene) (PVDF-HFP) as pellets, di-(2-ethylhexyl)phosphoric acid (DEHPA; 95%, Alfa Aesar, USA) and 2-nitrophenyl octyl ether (NPOE; 98%, Alfa Aesar, USA) were used for membrane casting (Fig. S2). The three acids: H_3PO_4, H_2SO_4 and HCl in different concentrations were used as receiving solutions.

Elements were incorporated in model solutions based on those commonly present in industrial acid wastes (Mg, Al, Sc, Ti, V, Cr, Mn, Fe, Y, Zr, Nb, La, Ce, Dy, Yb) (Hedwig et al., 2022; Remmen et al., 2019). Two solutions containing these elements in 0.1 mM or 1 mM concentrations with a pH of 1.5 were prepared. Model solution feeds were prepared from stock solutions of metal chlorides or oxides in hydrochloric acid (2 M). For pH adjustments a pH-meter (inoLab Multi 9310 IDS, WTW, Germany) was used.

The original acid waste came from the 'chloride route' of TiO_2 production and was provided by a manufacturer based in the Netherlands. Before the experiments, NaOH (98.5% purity) was added to adjust the pH to 1.5 and remove some of the impurities by precipitation (e.g. >99% Ti, 75% Th, 40% U; for details see Remmen et al., 2019 and Hedwig et al., 2022). After a settling period (48 h), the solids were removed by decantation and ultrafiltration (Molecular weight cut-off: 150 kDa, UP150, Microdyn-Nadir, Germany). Eventually a clear blue to green solution was obtained (for element concentrations see Table 5).

2.2. Membrane casting

The PIMs were cast using a solvent evaporation approach. PVDF-HFP, DEHPA and NPOE were dissolved in tetrahydrofuran by heating to reflux for 2 h, after which the solution was cooled to room temperature and an aliquot was poured into a glass ring (7.5 cm diameter) placed on a levelled float-glass table. The ring was covered with filter paper, and the solvent was allowed to evaporate overnight. Cast membranes were carefully peeled off the table. The membranes were weighed (KERN ABJ 320–4, Kern & Sohn, Germany), and their thickness was measured at five points using a micrometre screw gauge

Table 5
Initial concentrations and relative elemental distribution after 24 h of transport experiments using 7 M H_3PO_4 as receiving (elution) phase from real acid waste at 25 °C and 60 °C.

Element	c_0^{feed} [mmol L^{-1}]	Relative amount [%][a]					
		at 25 °C			at 60 °C		
		Feed	Membrane	Receiving phase	Feed	Membrane	Receiving phase
Li	0.26 ± 0.01	100 ± 20	0 ± 20	n.d.[b]	90 ± 20	10 ± 20	n.d.
Na	1190 ± 70	95 ± 5	5 ± 5	n.d.	99 ± 9	1 ± 9	n.d.
Al	100 ± 4	99 ± 4	1 ± 4	0.03 ± 0.01	100 ± 40	0 ± 40	0.1 ± 0.2
K	3.11 ± 0.1	95 ± 6	5 ± 6	n.d.	100 ± 7	0 ± 7	n.d.
Sc	0.94 ± 0.01	2 ± 1	70 ± 5	28 ± 5	0.2 ± 0.2	37 ± 8	63 ± 8
Ti	0.45 ± 0.01	83 ± 1	17 ± 1	0.2 ± 0.2	43 ± 3	47 ± 3	11 ± 2
V	19 ± 1	96 ± 5	3 ± 5	1.4 ± 0.1	100 ± 10	0 ± 10	2.6 ± 0.2
Cr	13 ± 1	97 ± 6	3 ± 6	n.d.	100 ± 30	0 ± 30	0.1 ± 0.2
Mn	66 ± 5	97 ± 6	3 ± 6	n.d.	95 ± 6	5 ± 6	0.04 ± 0.03
Fe	290 ± 20	97 ± 5	3 ± 5	0.05 ± 0.01	100 ± 7	0 ± 10	0.45 ± 0.06
Ni	0.82 ± 0.04	103 ± 1	0 ± 1	n.d.	96 ± 3	3 ± 3	1 ± 1
Zn	0.50 ± 0.01	107 ± 7	0 ± 8	3 ± 2	96 ± 8	4 ± 8	n.d.
Y	0.30 ± 0.01	87 ± 5	4 ± 5	9 ± 2	70 ± 8	13 ± 8	17 ± 3
Zr	0.11 ± 0.01	37 ± 2	62 ± 2	1 ± 1	28 ± 6	56 ± 7	16 ± 4
Nb	0.013 ± 0.001	33 ± 4	67 ± 4	n.d.	40 ± 4	49 ± 5	11 ± 2
Ba	0.73 ± 0.02	101 ± 3	0 ± 3	n.d.	100 ± 3	0 ± 3	0.9 ± 0.2
La	0.302 ± 0.002	101 ± 6	0 ± 6	n.d.	96 ± 2	4 ± 2	0.1 ± 0.3
Ce	0.77 ± 0.01	101 ± 4	0 ± 4	n.d.	94 ± 3	5 ± 3	0.7 ± 0.5
Pr	0.088 ± 0.001	101 ± 3	0 ± 3	n.d.	93 ± 2	6 ± 3	1.4 ± 0.5
Nd	0.312 ± 0.003	102 ± 3	0 ± 3	n.d.	91 ± 3	8 ± 3	1.8 ± 0.5
Sm	0.061 ± 0.002	100 ± 4	0 ± 4	n.d.	85 ± 5	9 ± 5	6.2 ± 0.9
Eu	0.010 ± 0.001	93 ± 3	7 ± 3	n.d.	84 ± 9	6 ± 9	10 ± 4
Gd	0.039 ± 0.001	94 ± 3	6 ± 3	n.d.	85 ± 5	5 ± 5	10 ± 2
Tb	0.007 ± 0.001	90 ± 3	10 ± 3	n.d.	80 ± 10	0 ± 20	17 ± 5
Dy	0.037 ± 0.001	89 ± 3	11 ± 3	n.d.	76 ± 4	5 ± 4	20 ± 3
Ho	0.008 ± 0.001	85 ± 4	15 ± 4	n.d.	78 ± 7	2 ± 7	20 ± 3
Er	0.023 ± 0.001	84 ± 5	16 ± 5	n.d.	73 ± 6	7 ± 6	21 ± 3
Tm	0.004 ± 0.001	82 ± 6	18 ± 6	n.d.	67 ± 6	9 ± 7	24 ± 3
Yb	0.027 ± 0.001	74 ± 8	20 ± 9	6 ± 3	67 ± 7	0 ± 7	34 ± 3
Lu	0.005 ± 0.001	70 ± 8	30 ± 8	n.d.	55 ± 7	18 ± 7	27 ± 3
Pb	0.144 ± 0.003	99 ± 3	1 ± 3	n.d.	94 ± 3	6 ± 4	n.d.
Th	0.063 ± 0.001	11 ± 8	61 ± 9	28 ± 5	2 ± 2	32 ± 7	66 ± 7
U	0.002 ± 0.001	82 ± 4	18 ± 4	n.d.	10 ± 30	90 ± 20	n.d.

[a] Relative amount: Feed $= \frac{c_{24h}^{feed}}{c_0^{feed}} \times 100\%$; Membrane $= 100\ \% - \text{Feed} - \text{Receiving phase}$; Receiving phase $= \frac{c_{24h}^{rec}}{c_0^{feed}} \times 100\%$.
[b] n.d. = not detected (< detection limit, see SI).

(Micromaster, 0–30 mm, TESA, Switzerland).

2.3. Extraction and elution experiments

For extraction and elution experiments, rectangular pieces (15 × 30 mm) were punched out of a PIM and fixed in 3D-printed polypropylene (PP) frames (Fig. S3). The PIMs thus prepared were immersed in a feed solution (0.1 mM, 40 mL) and shaken at 300 rpm and 25 °C in a thermo-shaker (IKA, KS 4000 i control, Germany) for 24 h. Afterwards, the PIMs were removed from the solution, dried with a paper tissue, fixed again in a PP frame and immersed in a receiving solution (40 mL; 300 rpm; 25 °C). The loading capacity Q_M (i.e. the absolute amount of a metal M extracted per membrane; µmol g^{-1}), was determined after 24 h when the metal uptake had reached a plateau. Furthermore, χ_M (i.e. the mole fraction of a metal M among the extracted metals) and $J_{0,M}$ (i.e. the initial flux of a metal M; nmol m^{-2} s^{-1}) were calculated (for calculations see SI). The latter was determined via the rate constant of the extraction k_{ex}, whereas for the elution, the rate constant was denoted as k_{el} (calculations in SI). As a control test to account for equipment-related sorption, one set of triplicates was run without any PIM.

2.4. Transport experiments

Transport experiments were conducted using custom-made high-density polyethylene (HDPE) cells (Fig. S3). Every cell consisted of two connectable half-cells, each holding 120 mL. The junction between them was circular (20 cm^2). The PIMs were inserted between the half cells, which were then filled with feed and receiving solution. Cells were agitated at 300 rpm in a thermo-shaker, if not otherwise stated, at 25 °C (IKA, KS 4000 i control, Germany).

2.5. Design of experiments

To find the optimal ratios of PVDF-HFP, DEHPA and NPOE while limiting the number of experiments, a DoE approach using STAVEX (AICOS Technologies AG, Switzerland) was used. Three response variables were defined to characterise an optimal PIM in terms of Sc extraction: 1) a high Sc loading capacity Q_{Sc}, 2) a high initial Sc extraction flux $J_{0,Sc}$ and 3) a high mole fraction of Sc among all extracted metals χ_{Sc}. The limits for the DoE were set as ω(PVDF-HFP) 25–95%, ω(DEHPA) 5–51% and ω(NPOE) 0–25%, respectively, where ω is the mass fraction of the corresponding constituent. The experimental plan was generated based on a D-optimal vertex-centroid design (Atkinson et al., 2001). In total, 11 different compositions, distributed over the entire factor region, were specified by the software. The corresponding membranes were cast and used for extraction experiments (duplicate, 24 h, 0.1 mM model feed). Based on the empirical data, the software fitted statistical models for each response variable, expressing how the response depends on the three influence factors. The *p*-values of the model parameters express the probability that a parameter has a

significant influence on the response variable.

2.6. QqQ-ICP-MS analysis

The samples were diluted using 3% nitric acid using an autodilution system (Simprep, Teledyne Cetac Technologies, USA) and analysed using triple quadrupole (QqQ) inductively coupled plasma mass spectrometry (ICP-MS). The analysis was performed on an 8800 QqQ-ICP-MS system (Agilent, Basel, Switzerland) using general purpose operational settings. Quantification was performed via multi-element standards (0–50 µg L^{-1} (ppb), seven points). To account for matrix effects, ^{103}Rh was used as the internal standard. To quantify $^{23}Na^+$, $^{52}Cr^+$, $^{55}Mn^+$, $^{56}Fe^+$, $^{60}Ni^+$, $^{66}Zn^+$, $^{89}Y^+$, $^{137}Ba^+$, $^{139}La^+$, $^{140}Ce^+$, $^{141}Pr^+$, $^{146}Nd^+$, $^{147}Sm^+$, $^{153}Eu^+$, $^{157}Gd^+$, $^{159}Tb^+$, $^{163}Dy^+$, $^{165}Ho^+$, $^{166}Er^+$, $^{169}Tm^+$, $^{172}Yb^+$, $^{208}Pb^+$, $^{232}Th^+$ and $^{238}U^+$, the ICP-MS was operated in single quad mode using helium as a collision gas, whereas $^{24}Mg^+$, $^{27}Al^+$, $^{39}K^+$, $^{45}Sc^+$, $^{47}Ti^+$, $^{51}V^+$, $^{90}Zr^+$ and $^{93}Nb^+$ were measured in triple-quad mass-shift mode using O_2 as a reaction gas. The $^7Li^+$ concentration was determined using no-gas single-quad mode (for figures of merit, see Table S2).

3. Results

3.1. Optimisation of the membrane composition

The optimisation approach was based solely on the extraction of metals from the feed into the PIM. In this regard, PIMs with a composition of 50/40/10 wt% PVDF-HFP/DEHPA/NPOE were found to provide the best compromise between Q_{Sc}, χ_{Sc} and $J_{0,Sc}$ while retaining structural integrity. At this optimal compromise composition, the statistical model predicted a Q_{Sc} of 117 ± 13 µmol g^{-1} (Fig. 1A; Table 1), χ_{Sc} of 0.37 ± 0.04 (Fig. 1B; Table 1) and $J_{0,Sc}$ of 150 ± 33 nmol m^{-2} s^{-1} (Fig. 1C; Table 1), respectively. The experimental results were largely consistent with this prediction (Table 1). Overall, the models described the experimental results well, reflected by the R^2 values of 95.3% (Q_{Sc}), 95.7% (χ_{Sc}) and 90.6% ($J_{0,Sc}$) (Table S3). The composition of 50/40/10 wt% PVDF-HFP/DEHPA/NPOE is henceforth referred to as 'optimal polymer inclusion membrane' (optimal PIM).

The scandium loading capacity (Q_{Sc}) increased with declining ω(PVDF-HFP) and rising ω(DEHPA), with ω(NPOE) having no visible effect (Fig. 1A). This stronger influence of ω(DEHPA) and ω(PVDF-HFP) compared to that of ω(NPOE) is also reflected by the non-significant p-values of the latter within the statistical model (Table S3). The optimal compromise PIM was already close to the best Q_{Sc} predicted at 45.8/42.6/11.7 wt% PVDF-HFP/DEHPA/NPOE (Table 1; Fig. 1A).

Co-extraction of other metals occurred each time, illustrated by a value of $\chi_{Sc} < 1$ (Fig. 1B; Tables 1 and 2). When using the optimal PIM, the overall selectivity and capacity order was Sc > Zr > Yb > Dy > Y > Ti > Ce > La > Fe > Al > Nb > V > Mn > Mg > Cr (Table 2). The maximum χ_{Sc} was calculated for a PIM composed of 88.3/4.5/7.2 wt% PVDF-HFP/DEHPA/NPOE (Fig. 1B). Here, all three factors were influential (Table S3).

With respect to $J_{0,Sc}$, a difference of one order of magnitude was calculated between the slowest and the fastest membranes (Fig. 1C; Table 1). The highest flux was achieved at 25/50/25 wt% PVDF-HFP/DEHPA/NPOE (Fig. 1C; Table 1), which was at the maximum of the DEHPA factor range and at the minimum of the PVDF-HFP factor range, consequently being almost at the minimum of the NPOE factor range. Based on the p-values within the statistical model, it seems that $J_{0,Sc}$ depends mainly on the linear effects of ω(DEHPA) and ω(PVDF-HFP), with the p-value of ω(NPOE) and for higher-order effects (interactions, quadratic terms) being insignificant.

The PIMs with PVDF-HFP content lower than 50% were not useable, since they showed strong adhesivity and were too soft to be removed from the glass table without damage, leading to the above specification of the optimal compromise setting.

3.2. Choice of receiving phase

Despite DEHPA having high selectivity for Sc extraction, the release from the membrane (elution) is challenging (Wang and Cheng, 2011; Yoshida et al., 2019b). Therefore, three mineral acids in different concentrations were tested as the receiving phase for Sc recovery from loaded PIMs. The best receiving phase for Sc elution was phosphoric acid (7–12 M), eluting >97 ± 5% of Sc (Fig. 2A).

Eluted Sc generally increased with higher acid concentration but was mostly dependent on the acid type (Fig. 2A). Phosphoric acid eluted a minor fraction of Sc at lower concentrations (2.7 ± 0.7% for 2 M), while it became considerably more effective when higher concentrations were used (61 ± 3% for 5 M, quantitative for >7 M). This was different to other acids: no elution for Sc using hydrochloric acid was found even at high molarities (1.0 ± 0.4% for 12 M), and H_2SO_4 resulted in a maximum elution of only 70 ± 9% when the highest concentration (12 M) was used (Fig. 2A). Furthermore, the membranes tended to be coloured yellow and red after contact with concentrated hydrochloric acid and sulfuric acid, respectively, suggesting instability issues. However, some preliminary IR data pointed towards stability at room temperature when using 7 M H_3PO_4 (Fig. S4). The stability of membranes for re-use applications in different acid media thus warrants further investigations.

Some co-extracted metals, such as the heavy rare earth elements, were easier to elute. Elution worked to some extent with all tested acids, as shown for Y (Fig. 2B). Quantitative results were achieved using

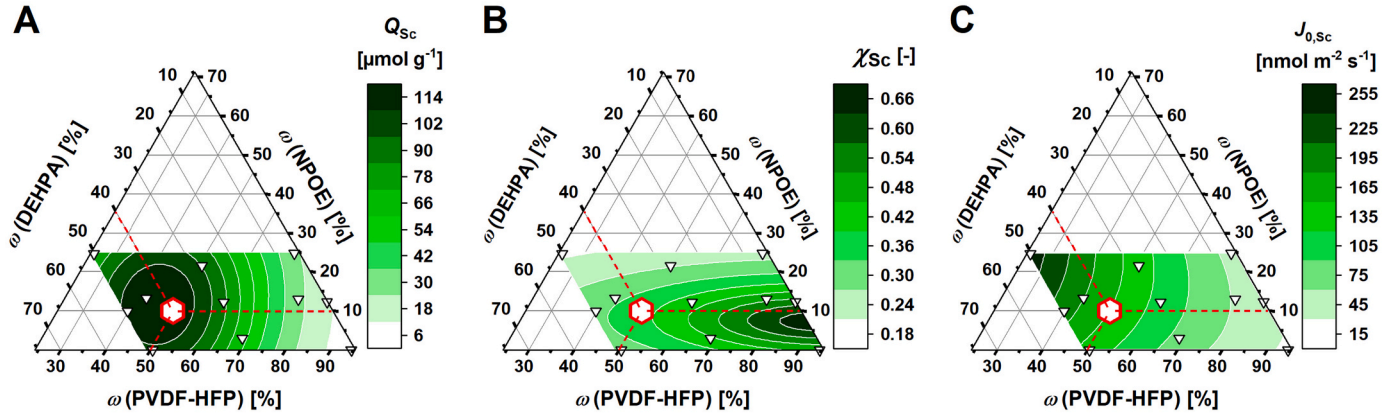

Fig. 1. DoE models for Sc loading capacity (Q_{Sc}; A), the mole fraction of Sc among all extracted metals (χ_{Sc}; B) and the initial flux of Sc extraction ($J_{0,Sc}$; C), used for membrane composition optimisation. White triangles indicate cast PIMs for verification, whereas the red dashed lines intersect at the optimal compromise between the three parameters. (For interpretation of the references to colour in this figure legend, the reader is referred to the web version of this article.)

Table 1
Modelled and measured results of the DoE study on extraction tests with model feed (15 elements, each 0.1 mM).

Membrane composition			Modelled			Measured (%-predicted)[a]			
ω(PVDF-HFP) [%]	ω(DEHPA) [%]	ω(NPOE) [%]	Q_{Sc} (± 13) [μmol g^{-1}]	χ_{Sc} (± 0.04) [−]	$J_{0,Sc}$ (± 33) [nmol m^{-2} s^{-1}]	Q_{Sc} [μmol g^{-1}]	χ_{Sc} [−]	$J_{0,Sc}$ [nmol m^{-2} s^{-1}]	Sc extracted [%][b]
95	5	0	6	0.46	26	6 ± 7 (95)	0.07 ± 0.12 (15)	2 ± 1 (8)	3 ± 4
83	5	12	14	0.54	40	13 ± 7 (88)	0.50 ± 0.49 (93)	40 ± 11 (101)	8 ± 5
76	11	13	28	0.49	57	36 ± 5 (131)	0.55 ± 0.44 (111)	89 ± 20 (155)	16 ± 2
70	5	25	26	0.24	47	28 ± 7 (107)	0.25 ± 0.17 (103)	51 ± 12 (108)	14 ± 3
69	28	3	64	0.44	83	72 ± 5 (112)	0.45 ± 0.16 (103)	111 ± 25 (134)	32 ± 2
60	28	12	86	0.42	110	75 ± 4 (86)	0.40 ± 0.14 (95)	114 ± 25 (103)	37 ± 2
51	28	21	96	0.27	134	83 ± 7 (86)	0.27 ± 0.06 (99)	91 ± 34 (68)	29 ± 3
50	50	0	105	0.30	137	104 ± 6 (99)	0.29 ± 0.07 (99)	142 ± 51 (103)	44 ± 3
50	40	10	117	0.37	150	95 ± 8 (81)	0.29 ± 0.03 (78)	136 ± 17 (91)	48 ± 4
43	44	13	118	0.32	181	133 ± 21 (113)	0.31 ± 0.08 (96)	177 ± 27 (98)	38 ± 6
40	50	10	111	0.31	192	101 ± 7 (91)	0.33 ± 0.1 (105)	166 ± 68 (87)	58 ± 4
25	50	25	73	0.20	257	78 ± 1 (106)[c]	0.20 ± 0.03 (100)	283 ± 15 (110)	76 ± 1

[a] $\%-\text{predicted} = \frac{\text{value (measured)}}{\text{value (modelled)}}$

[b] $\text{Sc extracted} = \left(1 - \frac{c_{24h}^{feed}}{c_0^{feed}}\right) \times 100\%$

[c] The membrane was cast twice as thick due to stability issues

hydrochloric acid and phosphoric acid at concentrations ≥7 M and sulfuric acid at 12 M.

The lowest phosphoric acid concentration that still yielded quantitative Sc elution was 7 M H_3PO_4 (Fig. 2A), and this was deemed the optimal receiving phase for transport experiments, despite some co-extracted metals (e.g. Y; 94 ± 6%).

3.3. Sc transport from model solutions

In transport experiments using 0.1 mM model solutions, Sc was efficiently transported into the membrane (91 ± 2%; Fig. 3A). The fraction of Sc transported into the receiving phase was relatively high (48 ± 9%; Fig. 3B); however, this was opposed by a poor selectivity. Scandium(III) was the metal ion of the third-lowest concentration in the receiving phase under these conditions (Fig. 3B, Table 3). In contrast to Sc(III), Y(III) was twice as fast extracted and quantitatively transported into the receiving phase (Fig. 3B, Table 3).

Using concentrated model solutions (1 mM), most Sc was transported into the membrane (Fig. 3C; Table 4) and one third of the total Sc was eluted into the receiving phase both within 24 h (Fig. 3D; Table 4). Selectivity for Sc was high, reaching the highest χ_{Sc} among the elements in the phosphoric acid after 24 h (Fig. 3B; Table 4). Other metals in the receiving phase were Yb, Y, Dy and smaller traces of Ti, V, La and Ce (Table 4). Regarding the kinetics, the highest k_{ex} and $J_{0,M}$ were obtained for Sc, with $J_{0,Sc}$ being ten times higher than in the experiments with diluted model solutions (Fig. 3A; Table 4). The increase in $J_{0,Sc}$, is in accordance with the linear proportionality of $J_{0,M}$ to c_0^{feed} (eq. 4, SI). Still, k_{ex} for Sc was around 17% lower than in experiments with 0.1 mM model solutions. Differences in the transport kinetics after the feed change were more sizable for other elements. Here, $J_{0,M}$ of co-transported metals were at least one order of magnitude lower than $J_{0,Sc}$ (Fig. 3C and D; Table 4).

In terms of Sc elution, k_{el} (0.019 ± 0.001 h^{-1}) was found to be 10 times lower than the corresponding k_{ex} (Fig. 3C and D; Table 4). In contrast, for Y with a k_{el} of 0.04 ± 0.02 h^{-1}, the rate constant was around four times greater than the corresponding k_{ex} (Fig. 3C and D; Table 4).

3.4. Sc transport from real acid waste

Scandium(III) was transported quantitatively (Fig. 4C; Table 5) into the membrane when using real waste as a feed for the optimised PIM, making it the most extracted element among all elements measured (Fig. 4C; Table 5). Only a few elements showed similarly high transport (Fig. 4C; Table 5). Around one third of the Sc was eluted into the receiving phase within 24 h (Fig. 4D; Table 5). Notably, χ_{Sc} increased by a factor of 600 from (5.6 ± 0.3) x10^{-4} in the feed to 0.34 ± 0.7 in the receiving phase (Table S4). In terms of co-transport, Th and Y were also significantly eluted into the receiving phase (Fig. 4D; Table 5). However, because of their lower c_0^{feed}, Th and Y added little to the total amount of transported metal (χ_{Th}: 0.023 ± 0.004 and χ_Y: 0.04 ± 0.01; Fig. 4B; Table S4). Instead, metals with high c_0^{feed} in the acid waste were associated with Sc in the receiving phase: V (χ_V: 0.34 ± 0.04), Fe (χ_{Fe}: 0.19 ± 0.04) and Al (χ_{Al}: 0.042 ± 0.007; Fig. 4B; Table S4). All other metals had $\chi_M < 0.01$ (Fig. 4B; Table S4).

In terms of kinetics, for Sc, a $J_{0,Sc}$ of 3500 ± 300 nmol m^{-2} s^{-1} was determined, along with a k_{ex} of 0.22 ± 0.02 h^{-1}. In comparison, for Th, a k_{ex} of 0.14 ± 0.02 h^{-1} but 25 times lower flux $J_{0,Th}$ with 140 ± 20 nmol m^{-2} s^{-1} was calculated. Yttrium(III) had a relatively lower rate constant k_{ex} of 0.03 ± 0.01 h^{-1} but a $J_{0,Y}$ of 160 ± 60 nmol m^{-2} s^{-1}, which was similar to Th, due to five times higher c_0^{feed} of Y (Table 5). As in the transport experiments using model feed, Sc elution was considerably slower than extraction by the membrane. A k_{el} of 0.015 ± 0.001 h^{-1} was found for Sc. For Th, a k_{el} of 0.012 ± 0.001 h^{-1}, and for Y, a k_{el} of 0.056 ± 0.005 h^{-1}, were determined.

Table 2
Mean Q_M, X_M and $J_{0.M}$ after 24 h extraction using the optimal PIM and model feed.

Element	c_0^{feed} [mmol L^{-1}]	c_{24}^{feed} [mmol L^{-1}]	Extracted [%][a]	Q_M [µmol g^{-1}]	X_M [−]	$J_{0,M}$ [nmol m^{-2} s^{-1}]
Sc	0.092 ± 0.001	0.048 ± 0.001	48 ± 4	95 ± 8	0.29 ± 0.03	140 ± 20
Zr	0.085 ± 0.002	0.066 ± 0.002	21 ± 2	39 ± 3	0.12 ± 0.01	70 ± 20
Yb	0.089 ± 0.001	0.073 ± 0.001	17 ± 2	32 ± 3	0.10 ± 0.01	61 ± 4
Dy	0.087 ± 0.002	0.075 ± 0.002	14 ± 1	26 ± 1	0.08 ± 0.01	52 ± 8
Y	0.085 ± 0.001	0.074 ± 0.001	13 ± 1	23 ± 1	0.07 ± 0.01	53 ± 9
Ti	0.097 ± 0.002	0.085 ± 0.002	11 ± 4	23 ± 9	0.07 ± 0.02	50 ± 30
Ce	0.086 ± 0.001	0.076 ± 0.001	11 ± 1	20 ± 2	0.06 ± 0.01	30 ± 10
La	0.060 ± 0.001	0.052 ± 0.001	12 ± 1	16 ± 1	0.05 ± 0.01	23 ± 7
Fe	0.052 ± 0.005	0.045 ± 0.005	13 ± 9	14 ± 9	0.04 ± 0.03	20 ± 30
Al	0.061 ± 0.004	0.055 ± 0.004	9 ± 4	11 ± 6	0.04 ± 0.01	7 ± 5
Nb	0.036 ± 0.001	0.030 ± 0.001	14 ± 2	10 ± 2	0.03 ± 0.01	40 ± 3
V	0.067 ± 0.003	0.064 ± 0.003	4 ± 2	6 ± 3	0.02 ± 0.01	40 ± 20
Mn	0.068 ± 0.002	0.065 ± 0.002	3 ± 2	5 ± 3	0.01 ± 0.01	15 ± 10
Mg	0.057 ± 0.003	0.055 ± 0.003	3 ± 2	4 ± 3	0.01 ± 0.01	8 ± 7
Cr	0.071 ± 0.002	0.070 ± 0.002	1 ± 1	1 ± 1	0.00 ± 0.01	14 ± 6

[a] $\text{Extracted} = \left(1 - \frac{c_{24h}^{feed}}{c_0^{feed}}\right) \times 100\%$

3.4.1. Influence of temperature

When the temperature was increased to 60 °C, virtually all Sc was transported into the membrane (Fig. 5A; Table 5). In comparison to the experiments at 25 °C, more co-transport of other elements occurred (Fig. 5A; Table 5). Sc transport was significantly more effective at higher temperature, with approx. twice as much Sc eluted into the receiving phase compared to room temperature (Table 5). χ_{Sc} was relatively high in the receiving phase, with a value of 0.18 ± 0.02 (Table S5). Nevertheless, more co-transportation of other metals occurred (Fig. 5A–5D; Table 5). Thorium and the heavy rare earth elements were particularly increased in the receiving phase (Table 5). However, as c_0^{feed} for these competing elements was substantially smaller than for Sc, their contribution to the total amount of transported substance was small (Fig. 5B; Table 5). In absolute numbers, the most prevalent impurities transported were Fe and V, as already observed in the experiments at room temperature (Fig. 5B; Table 5). Iron in particular showed a steep concentration gain, which began after ca. 5 h of operation. Hence, χ_{Fe} reached 0.5 ± 0.1 and χ_V was 0.18 ± 0.03 after 24 h in the receiving phase (Table S5). Extraction kinetics were increased by as much as a factor of 2.5 ($J_{0,Sc}$ = 8000 ± 100 nmol m^{-2} s^{-1}; k_{ex} = 0.54 ± 0.01 h^{-1}). For Sc elution, a k_{el} of 0.043 ± 0.001 h^{-1} was determined, which was almost three times higher than in the 25 °C experiments. In contrast, a k_{ex} of 0.34 ± 0.02 h^{-1} and a $J_{0,Th}$ of 310 ± 20 nmol m^{-2} s^{-1} were determined for Th. However, Th was slightly faster eluted than Sc, with a k_{el} of 0.046 ± 0.003 h^{-1}.

4. Discussion

4.1. Optimisation of membrane/receiving phase

The membrane composition was optimised by means of an extraction/elution approach, optimising metal uptake into the membrane (extraction) and metal release from the membrane (elution) separately. For extraction, the optimal PIM was composed of 50/40/10 wt% PVDF-HFP/DEHPA/NPOE and harvested most Sc (Q_{Sc} = 95 ± 8 µmol g^{-1}) at a higher velocity ($J_{0,Sc}$ = 140 ± 20 nmol m^{-2} s^{-1}) and acceptable selectivity over other elements (χ_{Sc} = 0.29 ± 0.03). Ideally, all three parameters should be maximised, yet χ_{Sc} behaved oppositely to Q_{Sc} and $J_{0,Sc}$: while Q_{Sc} and $J_{0,Sc}$ increased with increasing DEHPA/decreasing polymer content of the membrane, χ_{Sc} did not. Since metal extraction is based on a chemical reaction between the carrier and the metal, higher carrier concentration can lead to higher reaction rates and a larger $J_{0,Sc}$. The Q_{Sc}, on the other hand, may benefit from increasing carrier concentration due to the higher number of binding sites available in the PIM. However, with more binding sites, more co-extraction may occur once the total capacity is sufficient to absorb not only the bulk of Sc but also metals with lower affinity for DEHPA. Furthermore, the reaction rates for the complexation of competing metals by DEHPA may benefit similarly to the complexation of Sc when the concentration of the carrier is increased. Together, these effects could explain the opposite influences of increasing DEHPA concentration on $J_{0,Sc}$, Q_{Sc} and χ_{Sc}. In this study, the optimal PIM was defined with respect to the maximum Sc yield at the expense of some selectivity. Once extracted and

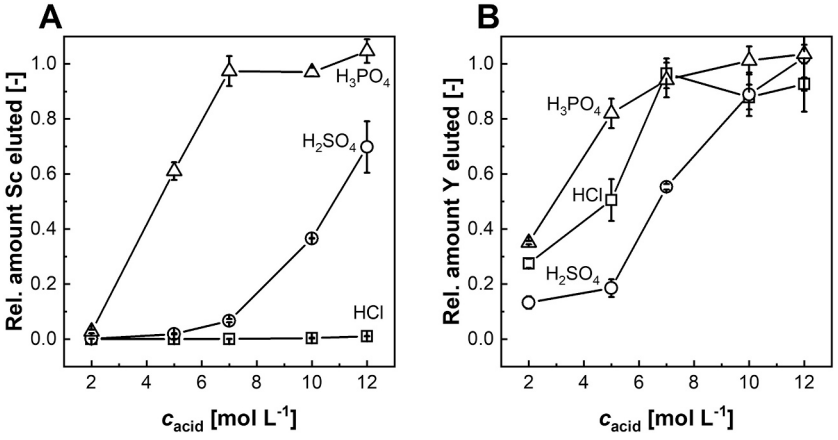

Fig. 2. Relative eluted Sc (A) and Y (B) at different receiving phases.

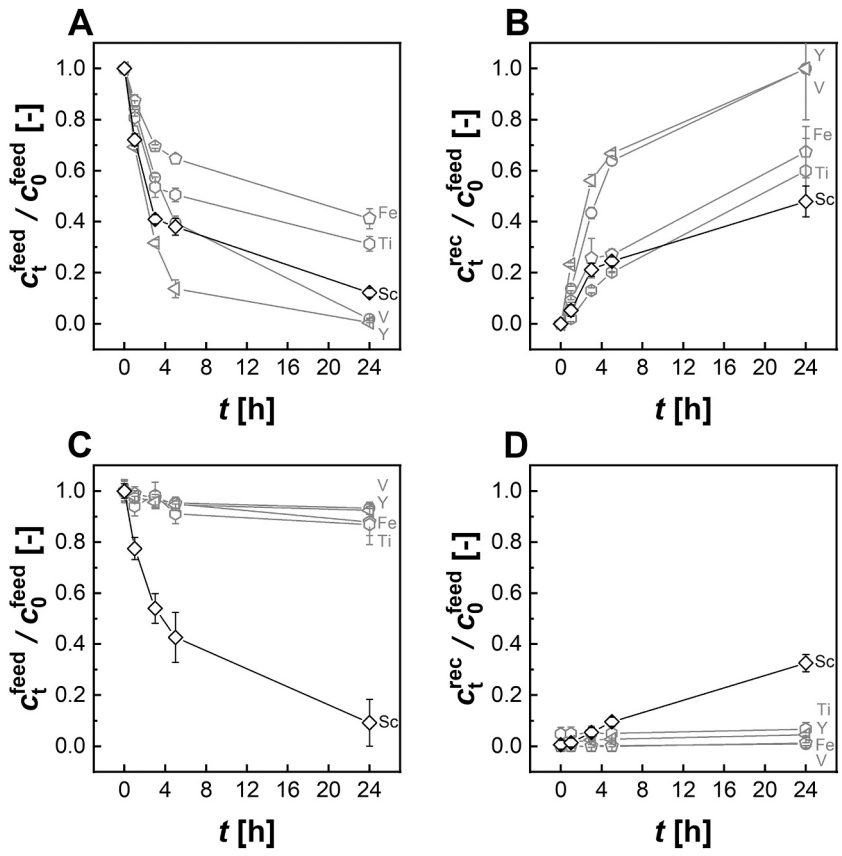

Fig. 3. Extraction kinetics of transport experiments using 7 M H_3PO_4 as receiving phase from 0.1 mM (A, B) and 1 mM (C, D) multi-element feed with the concentration of the feed side (A,C) and the receiving side (B, D).

Table 3
Results after 24 h transport experiments using 7 M H_3PO_4 as receiving (elution) phase from 0.1 mM model feed.

		Relative amount [%][a]						
Element	c_0^{feed} [mmol L^{-1}]	Feed	Membrane	Receiving phase	χ_M^{rec} [−]	k_{ex} [h^{-1}]	P [mm h^{-1}]	$J_{0,M}$ [nmol m^{-2} s^{-1}]
Mg	0.12 ± 0.02	92 ± 7	0 ± 10	20 ± 10	0.02 ± 0.01	0.02 ± 0.01	1.3 ± 0.6	50 ± 30
Al	0.11 ± 0.01	34 ± 3	0 ± 20	90 ± 20	0.10 ± 0.01	0.03 ± 0.01	1.6 ± 0.6	60 ± 20
V	0.10 ± 0.01	1 ± 1	0 ± 20	100 ± 20	0.10 ± 0.01	0.19 ± 0.02	11.2 ± 0.7	320 ± 30
Cr	0.11 ± 0.01	78 ± 3	0 ± 5	26 ± 5	0.02 ± 0.01	0.01 ± 0.01	0.5 ± 0.3	10 ± 10
Mn	0.11 ± 0.01	60 ± 5	0 ± 20	40 ± 20	0.04 ± 0.01	0.02 ± 0.01	1.1 ± 0.2	30 ± 10
Fe	0.12 ± 0.01	41 ± 4	0 ± 20	60 ± 20	0.07 ± 0.01	0.09 ± 0.01	5.3 ± 0.3	180 ± 20
Sc	0.07 ± 0.01	12 ± 2	40 ± 7	48 ± 7	0.03 ± 0.01	0.20 ± 0.02	12 ± 1	260 ± 20
Ti	0.11 ± 0.01	31 ± 3	10 ± 20	50 ± 20	0.06 ± 0.01	0.14 ± 0.02	8.5 ± 0.8	270 ± 40
Y	0.11 ± 0.01	0 ± 20	0 ± 30	100 ± 20	0.11 ± 0.01	0.40 ± 0.05	24 ± 3	800 ± 90
Zr	0.08 ± 0.01	70 ± 20	20 ± 20	0 ± 10	0.00 ± 0.01	0.00 ± 0.02	0 ± 2	0 ± 30
Nb	0.06 ± 0.01	100 ± 30	0 ± 30	0 ± 10	0.00 ± 0.01	0.00 ± 0.02	0 ± 1	0 ± 20
La	0.11 ± 0.01	0 ± 1	0 ± 20	90 ± 20	0.10 ± 0.01	0.25 ± 0.03	15 ± 2	500 ± 100
Ce	0.11 ± 0.01	0 ± 1	0 ± 20	90 ± 20	0.10 ± 0.01	0.29 ± 0.03	17 ± 2	600 ± 100
Dy	0.15 ± 0.01	0 ± 1	0 ± 20	100 ± 20	0.15 ± 0.01	0.39 ± 0.05	23 ± 3	1000 ± 200
Yb	0.11 ± 0.01	0 ± 1	0 ± 20	100 ± 20	0.10 ± 0.01	0.44 ± 0.06	27 ± 4	870 ± 100

[a] Relative amount: Feed $= \frac{c_{24h}^{feed}}{c_0^{feed}} \times 100\%$; Membrane $= 100\ \% - \text{Feed} - \text{Receiving phase}$; Receiving phase $= \frac{c_{24h}^{rec}}{c_0^{feed}} \times 100\%$

concentrated from the ppm level present in waste (Remmen et al., 2019), selectivity can still be achieved during purification and refining, for example by liquid–liquid extraction and/or ion exchange (Avdibegović et al., 2019; Wang et al., 2011; Wang and Cheng, 2011). However, according to the DoE results, PIM selectivity could be improved to some degree through the addition of NPOE in exchange for DEHPA. Generally, the role of the plasticiser is to weaken the interactions between the polymer chains, which in turn makes the membrane softer and more flexible. In addition, the carrier mobility within the PIM can be increased, which is important for metal transport through the membrane (Nghiem et al., 2006). In this study, 5–10 wt% NPOE was found to improve Sc extraction selectivity. This was particularly pronounced in PIMs with lower DEHPA content. From the empirical model of the experimental results (see SI), the membrane composition for the highest selectivity could be identified (88.3/4.5/7.2 wt% PVDF-HFP/DEHPA/NPOE). This could be advantageous for obtaining a purer Sc content in an earlier step (the receiving phase) of the processing chain. Due to the considerable Sc losses, however, it is

Table 4
Results after 24 h transport experiments using 7 M H_3PO_4 as receiving (elution) phase from 1 mM model feed.

		Relative amount [%][a]						
Element	c_0^{feed} [mmol L^{-1}]	Feed	Membrane	Receiving phase	χ_M^{rec} [−]	k_{ex} [h^{-1}]	P [mm h^{-1}]	$J_{0,M}$ [nmol m^{-2} s^{-1}]
Mg	0.9 ± 0.1	93 ± 6	7 ± 6	0 ± 2	0.00 ± 0.05	0.012 ± 0.006	0.7 ± 0.3	160 ± 80
Al	1.1 ± 0.1	94 ± 3	6 ± 4	0 ± 2	0.00 ± 0.04	0.006 ± 0.01	0.3 ± 0.6	110 ± 200
V	0.8 ± 0.1	93 ± 2	6 ± 2	1 ± 1	0.02 ± 0.02	0.008 ± 0.004	0.5 ± 0.2	110 ± 50
Cr	1.0 ± 0.1	96 ± 3	4 ± 3	0 ± 1	0.00 ± 0.02	0.004 ± 0.003	0.2 ± 0.2	60 ± 60
Mn	1.2 ± 0.1	95 ± 3	5 ± 3	0 ± 1	0.00 ± 0.02	0.00 ± 0.01	0.0 ± 0.5	0 ± 200
Fe	1.0 ± 0.1	88 ± 5	11 ± 6	1 ± 2	0.00 ± 0.02	0.010 ± 0.005	0.6 ± 0.3	150 ± 90
Sc	0.7 ± 0.1	9 ± 9	60 ± 10	33 ± 3	0.60 ± 0.06	0.17 ± 0.04	10 ± 3	2000 ± 500
Ti	0.6 ± 0.1	87 ± 8	6 ± 8	7 ± 3	0.03 ± 0.02	0.02 ± 0.01	1.3 ± 0.7	200 ± 100
Y	1.0 ± 0.1	92 ± 2	3 ± 2	5 ± 1	0.10 ± 0.02	0.011 ± 0.002	0.6 ± 0.1	170 ± 30
Zr	0.4 ± 0.1	90 ± 9	0 ± 9	10 ± 2	0.00 ± 0.01	0.01 ± 0.01	0.8 ± 0.7	80 ± 70
Nb	0.4 ± 0.1	100 ± 40	0 ± 40	2 ± 3	0.00 ± 0.01	0.00 ± 0.05	0 ± 3	0 ± 200
La	0.9 ± 0.1	97 ± 2	3 ± 2	0.8 ± 0.3	0.01 ± 0.01	0.006 ± 0.004	0.3 ± 0.3	80 ± 60
Ce	0.7 ± 0.1	97 ± 2	2 ± 2	1.1 ± 0.4	0.01 ± 0.01	0.004 ± 0.002	0.3 ± 0.1	50 ± 20
Dy	0.9 ± 0.1	95 ± 2	2 ± 2	3 ± 1	0.08 ± 0.01	0.005 ± 0.002	0.3 ± 0.1	70 ± 40
Yb	1.0 ± 0.1	90 ± 2	4 ± 3	6 ± 2	0.15 ± 0.02	0.011 ± 0.004	0.7 ± 0.3	170 ± 70

[a] Relative amount: Feed $= \frac{c_{24h}^{feed}}{c_0^{feed}} \times 100\%$; Membrane $= 100\ \% - \text{Feed} - \text{Receiving phase}$; Receiving phase $= \frac{c_{24h}^{rec}}{c_0^{feed}} \times 100\%$

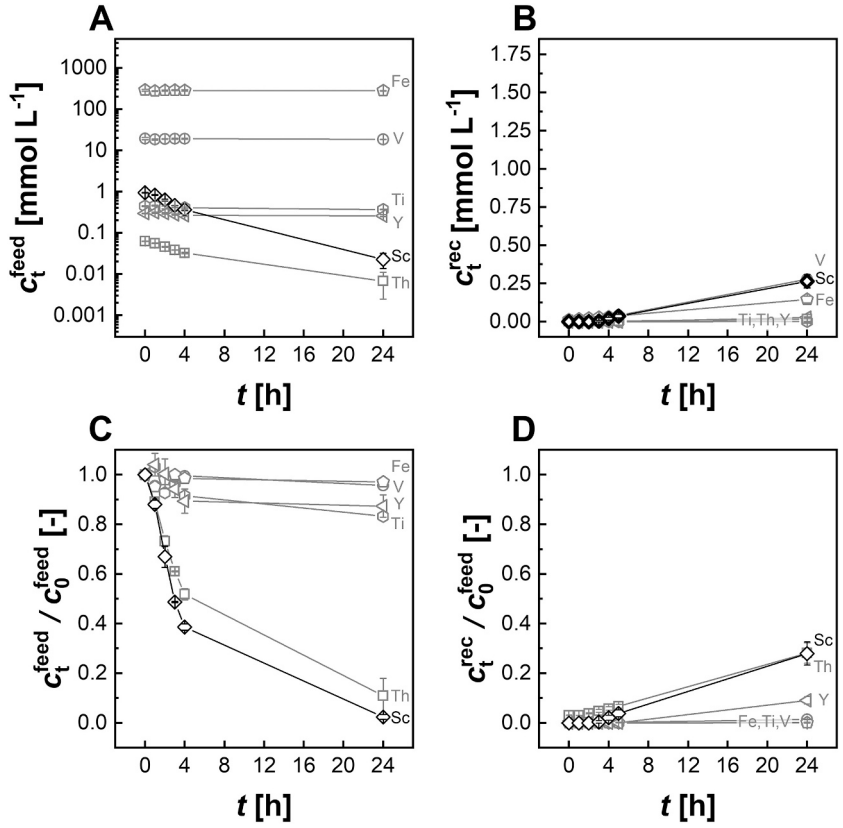

Fig. 4. Recovery of Sc from real acid waste feed (A, C) into 7 M H_3PO_4 receiving phase (B, D) in terms of absolute concentrations (top) and relative amounts (bottom) at 25 °C.

doubtful whether this would be acceptable for Sc recovery applications. Rather, it may be an interesting option for Sc selective electrodes (Almeida et al., 2017).

Another part of the optimisation was the identification of a suitable receiving phase. Due to the high affinity of DEHPA for Sc, the stripping of the loaded DEHPA phase is known to be problematic in conventional SX, where strong bases are needed (Wang and Cheng, 2011). However, the metal transport across the PIM relies on a proton gradient from the receiving to the feed phase, working as a driving force for the process (Nghiem et al., 2006). For this reason, only acids were considered as receiving phases. Here, H_3PO_4 turned out to be an exceptional medium, reaching >97 ± 5% for the Sc elution. This is remarkable, because HCl and H_2SO_4 were found to be relatively ineffective for elution, as previously identified in conventional SX studies using DEHPA (Ditze and Kongolo, 1997; Ochsenkühn-Petropulu et al., 1995; Pei et al., 2011). We assume that the advantage of phosphoric acid is based on the thermodynamically favoured formation of Sc phosphate complexes over sulfate and chloride complexes in the receiving phase (Wood and Samson, 2006). Due to their stability and low solubility products, Sc phosphates can be found naturally in mineral form (e.g. pretulite [$ScPO_4$] or

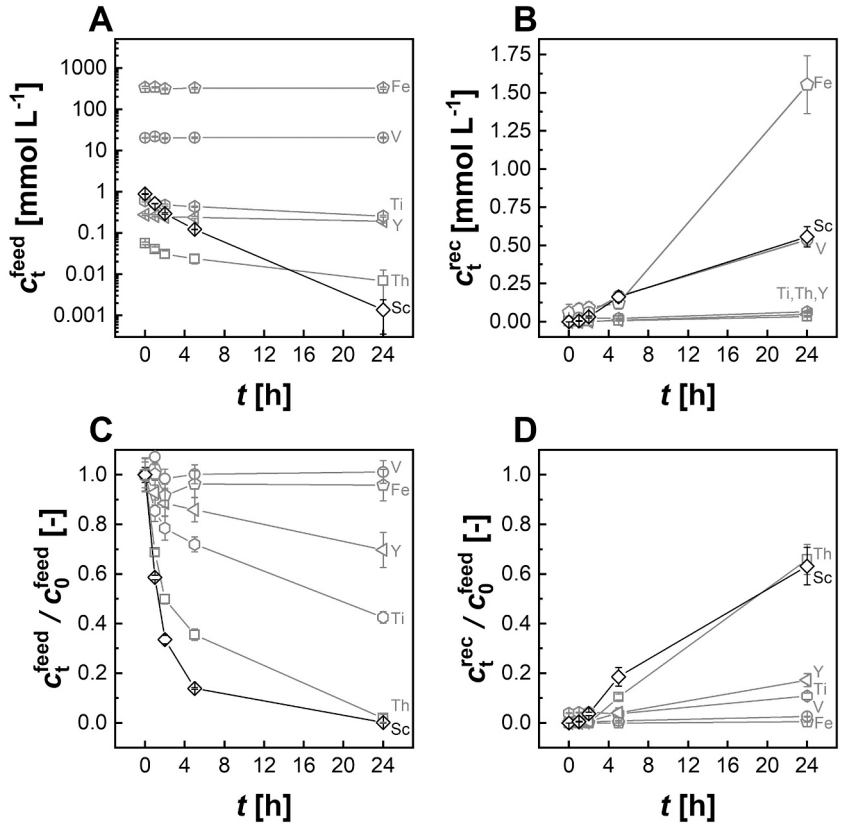

Fig. 5. Recovery of Sc from real acid waste feed (A, C) into 7 M H_3PO_4 receiving phase (B, D) in terms of absolute concentrations (top) and relative amounts (bottom) at 60 °C.

kolbeckite [$ScPO_4{\cdot}2H_2O$]) (Wood and Samson, 2006).

To the best of our knowledge, the recovery of Sc from a loaded organic DEHPA phase by means of phosphoric acid has not been reported, although the stripping potential of H_3PO_4 for uranium-loaded DEHPA has been described (Khorfan et al., 1998). Although the results were obtained with DEHPA-containing PIMs, they may be to some extent transferable to conventional SX, making H_3PO_4 an alternative to alkaline stripping (Li et al., 2018; Wang et al., 2011). For example, the addition of lye can lead to saponification of DEHPA, which causes stronger emulsion/poorer phase separation in SX (Sun et al., 2019; Wang et al., 1996; Wang and Cheng, 2011). This can lead to considerable extractant losses and eventually to the need to replace the organic phase (Sun et al., 2019; Wang et al., 1996; Wang and Cheng, 2011).

In comparison to co-extracted metals, Sc elution appears more challenging. On the one hand, this could be explained by the higher Lewis acidity of Sc and the stronger interaction between DEHPA and Sc, making the complex harder to cleave. On the other, it could also be a sign of different complexation of Sc and competing metals; the stoichiometry of the complex formed between lanthanides and DEHPA in PIMs is reported to be 1:6, consistent with complexation by DEHPA dimers (Croft et al., 2018; Nagul et al., 2019). In those studies, H_2SO_4 (0.3–7 M) was found to be a satisfactory receiving phase for the transport of lanthanides (La, Gd, Yb). In the case of Sc, a recent study found a metal-to-DEHPA ratio of 1:2.5, implying monomeric complexation of DEHPA (Das et al., 2018). It is unclear whether DEHPA binds to Sc as a monomer or dimer in the PIM (Fig. S5). Complexes of the monomer are expected to be less affected by ligand substitution and more difficult to cleave (Gajda and Bogacki, 2007). This may explain why HCl and H_2SO_4 were suitable for the elution of Y, for example, but not of Sc.

4.2. Sc recovery from model solutions and real waste

From 1 mM model feed solutions, Sc transport was selective and fast, using the optimal PIM and receiving phase (Fig. 3A and B, Table 4). In contrast, using the 0.1 mM model feed (Fig. 3C and D, Table 3), no selectivity could be observed, and most metals were transported equally fast. This implies that the affinity of DEHPA for Sc is not exceptionally high among the tested elements. It is unknown what exactly caused this change. One suggestion would be that different DEHPA-to-metal ratios may have led to this selectivity difference. In the case of the 1 mM feed, the ratio of DEHPA to metal was 2:5, while in the case of the 0.1 mM feed it was 12:5, considering differences in membrane thickness in the calculation. It is suggested that a lack of DEHPA compromises the formation of DEHPA-dimer complexes, or vice versa. Similarly, depending on the preferred coordination environment (1:3 or 1:6 metal:DEHPA; (Croft et al., 2018; Das et al., 2018; Nagul et al., 2019), the incorporation of a metal into the DEHPA-PIM may be hindered or accelerated. In the case of Sc, k_{ex} in both transport experiments were almost similar (0.17 ± 0.04 and 0.20 ± 0.02 h^{-1}). For Y, in contrast, k_{ex} was found to increase by almost 40 times when having a higher DEHPA/metal ratio (from 0.011 ± 0.003 h^{-1} to 0.40 ± 0.05 h^{-1}). Thus, a certain concentration of the feed solution may be mandatory to allow the proposed 'kinetic discrimination' mechanism and selective recovery of Sc. However, for dilute solutions, the DEHPA content of the membrane may then be reduced to limit the transport of other metals, which is in line with the decrease in χ_{Sc} with increasing DEHPA membrane content in the DoE model.

In comparison to the model solutions, the industrial acid waste contained more than twice as many elements that were non-equimolar

Table 6
Comparison of different studies, using PIMs for Sc recovery.

Carrier	$C_{0,Sc}^{feed}$ [mmol L^{-1}]	Feed solution	pH	$J_{0,Sc}$ [nmol m^{-2} s^{-1}]	Sc transported (24 h) [%]	Ref
benzoyltrifluoroacetone	0.5	0.1 M CH_3COOH/ CH_3COONa	6.1	690	–	(Sugiura et al., 1989)
2-thenoyltrifluoroacetone	0.5	0.1 M CH_3COOH/ CH_3COONa	6.1	610	–	(Sugiura et al., 1989)
2-furoyltrifluoroacetone	0.5	0.1 M CH_3COOH/ CH_3COONa	6.1	560	–	(Sugiura et al., 1989)
PC-88A & Versatic 10	0.1	0.1 M HNO_3/NH_4NO_3	4.0	190	35–40	(Sharaf et al., 2018)
N-[N,N-di(2-ethylhexyl) aminocarbonylmethyl] glycine	0.1	0.1 M $H_2SO_4/(NH_4)_2SO_4$	3.0	380	35–40	(Yoshida et al., 2019a)
N-[N,N-di(2-ethylhexyl)aminocarbonylmethyl] phenylalanine	0.1	0.1 M $H_2SO_4/(NH_4)_2SO_4$	3.0	180	35–40	(Yoshida et al., 2019a)
DEHPA	0.1	HCl (model solution)	1.5	260	48	This study
DEHPA	1	HCl (model solution)	1.5	2000	33	This study
DEHPA	1	HCl (TiO_2 acid waste, 25 °C)	1.5	3500	28	This study
DEHPA	1	HCl (TiO_2 acid waste, 60 °C)	1.5	8000	63	This study

concentrated. These 33 elements were present from mg L^{-1} to multiple g L^{-1} scale, while Sc accounted for only around 42 mg L^{-1} (~1 mM; Table 5). Nevertheless, Sc was still transported almost quantitatively into the membrane, and almost a third of the initial Sc was transported across the membrane into the receiving phase (Fig. 4A–4D; Table 5). Overall, a high selectivity was achieved, indicated by the increase of χ_{Sc} by a factor of 600 from the feed to receiving phase. Competing elements in terms of impurities co-transported were Y and Th. Although Th may generally be of occupational health and safety concern, here the final concentration was only 4.1 ± 0.7 ppm, which is below its average concentration in the Earth's crust (12 ppm) (Herring, 2012). Since the PIMs developed here could not discriminate between Th and Sc, downstream Th removal is necessary. This can be achieved by means of SX with neat tributyl phosphate (Wang and Cheng, 2011) or by simple pH adjustment, as shown previously in the original waste used here. With respect to Ti, some transport into the membrane was observed, while no considerable amount reached the receiving phase within 24 h (Fig. 4). While this underlined the successful separation of Ti and Sc with the PIM system, it also showed that Ti-rich feed solutions require pre-treatment as previously described.

Regarding the co-transport of major elements, satisfactory separation was achieved. In terms of Fe, only around 0.45% of the ca. 0.3 M Fe contained in the feed was transported into the receiving phase (Table 5). This suggested the presence of predominantly Fe(II), instead of Fe(III), as the former is poorly extracted by DEHPA only from chloride media (Bartkowska et al., 2002) and the 'chloride route' TiO_2 production comprises strongly reducing conditions (Bordbar et al., 2018), favouring Fe(II). The low Fe co-transport observed here is in contrast to Sc SX studies, reaching high (>98%) Sc extraction at the cost of higher (e.g. 6.21% (Gao et al., 2019), 10% (Ditze and Kongolo, 1997)) co-extraction of Fe. Similarly, ion exchange/solvent-impregnated resins found co-extraction of Fe (Wang et al., 2011), and our observations with PIMs represent a real advance in separation technology. For V, only 1.4% of the 20 mM were transported from the acid waste into the receiving phase (Table 5). Nevertheless, the two elements (V and Fe) account for >50% of the total elements in the receiving phase. Hence, further downstream removal/separation steps will be necessary to obtain a pure Sc product. It is possible that this may be achieved by selective precipitation either of Sc itself or impurities (Yagmurlu et al., 2017). In SX, such impurities could be removed after extraction by scrubbing/washing steps (Wang et al., 2011; Wang and Cheng, 2011).

However, regarding Sc elution from the loaded PIMs, there is room for improvement: whereas for SX, quantitative stripping from the loaded DEHPA phase appears achievable (Wang et al., 2011; Wang and Cheng, 2011), maximally 63 ± 7% of the membrane-bound Sc was eluted into the receiving phase (Fig. 5D).

Future implementation could involve scrubbing/washing steps instead of direct Sc elution to increase the selectivity of the process. As shown in Fig. 2, HCl or H_2SO_4 may be options for impurity removal, as they were ineffective in Sc elution from the membranes.

A further improvement in PIM Sc recovery would be increased transport velocity, resulting in lower contact times and a lower footprint. Here, the system was heated up to 60 °C, leading to twice as much Sc in the receiving phase after 24 h compared to the experiments at 25 °C. The PIM process crucially relies on diffusion (Almeida et al., 2017; Nghiem et al., 2006). Based on Fick's law and the Stokes–Einstein equation for the diffusion coefficient, increasing the temperature is anticipated to have two effects: 1) directly, through the linear proportionality of the diffusion coefficient to temperature and 2) indirectly, by reducing the viscosity, which is inversely proportional to temperature. Higher temperatures result in greater movement of the solutes and simultaneously less resistance of the medium. The latter could be particularly important for the diffusion across the membrane and also within the receiving phase (7 M H_3PO_4 is about four times as viscous as water at 25 °C (Shaltout et al., 2008)), facilitating the removal of transported Sc from the membrane surface.

The co-transport of other elements, such as Ti and Y was drastically increased (Fig. 5C and D; Table 5). However, absolute concentrations of these metals were typically an order of magnitude lower than of Sc or showed only little elution, such as Ti (Fig. 5A and B; Table 5). Thus, although 27 elements were found in the receiving phase, only two of them (Fe, V) accounted for 86% of all impurities (Table 5). Nevertheless, the increase of χ_{Sc} of over 300 times (from feed to receiving phase), underlined the selectivity for Sc.

All in all, these results suggest that the optimised system is a viable method for the extraction of Sc from industrial waste.

4.3. Comparison to previous PIM studies

The optimal PIM extraction conditions showed a high Sc flux of up to 44 times higher than in previous studies (Table 6). This is not due to the use of DEHPA but rather to the optimisation of experimental conditions. The initial Sc concentrations in the model solution and the acidic waste used for this study were 2–10 times higher than in other work, which increased the flux (Table 6; Eq. 4, SI). This study showed that PIMs can operate successfully even at pH <2 and that a buffered solution is not necessarily required.

Although it is mainly caused by higher initial concentrations, the possibility of drastically increasing the flux indicates that the potential of PIMs for Sc recovery has not yet been fully exploited and may be further optimised. It will be of interest to test streams with higher Sc concentrations for PIM-based Sc recovery in the future.

Another prerequisite for a functioning PIM system enabling metal transport is a functioning elution. As already described, Sc is notoriously difficult to cleave after complexation with phosphorus-based carriers. Yoshida et al. tested DEHPA as an extraction agent for Sc and excluded its use as a carrier for PIMs, as there were significant problems when trying to elute Sc with H_2SO_4 (Yoshida et al., 2019b). Similarly, Sharaf et al. reported difficulties for elution when using PC-88A as a carrier (Sharaf et al., 2018). In both studies, the carrier had to be changed/modified, to facilitate elution and successful Sc transport. By using H_3PO_4 as the receiving phase, we have demonstrated a way to use strong Sc complexing agents that are known to extract Sc even at very low pH. After 24 h, the transported Sc fractions in various transport experiments were of the same magnitude as in other studies (Table 6) (Sharaf et al., 2018; Yoshida et al., 2019a; Yoshida et al., 2019b).

4.4. Broader impact and implications for Sc recovery

In comparison to SX, PIMs reduce the amount of material needed by replacing the organic solvent phase with a thin polymer film, leading to the ecological footprint and costs arising from SX operation being mitigated (Vahidi and Zhao, 2016). This brings additional benefits by eliminating flammable solvents such as kerosene (Wang et al., 2011) during extraction. In our work, ca. 5 kg of membrane material was required to treat 1 m^3 of acid waste. Based on estimated prices for ton quantities (see SI), this translates into an investment of US$41 to recover Sc worth US$183 for a single cycle. Furthermore, PIMs can also be used in multiple cycles, and the surface-area-to-mass ratio can be further optimised. The energy demand for using PIMs does not differ considerably from that of SX or ion exchange, even though PIM Sc extraction worked best at 60 °C.

5. Conclusions

Although PIMs have been developed and optimised for decades (Nghiem et al., 2006), they have few, if any, commercial applications for metal recovery. PIM experiments related to metal recovery on a laboratory scale deal primarily with model solutions or streams (Almeida et al., 2012). In this paper, we have shown for the first time that PIMs allow highly selective metal separation from real industrial waste as an alternative to conventional SX or ion-exchange approaches. Using waste containing some 30 metals, some of which were present at multiple g L^{-1} concentrations, minute amounts (mg L^{-1}) of Sc were separated with efficiency and selectivity.

CRediT authorship contribution statement

Sebastian Hedwig: Conceptualization, Formal analysis, Investigation, Methodology, Project administration, Supervision, Validation, Visualization, Writing – original draft, Writing – review & editing. **Manuel Kraus:** Formal analysis, Investigation, Validation. **Meret Amrein:** Formal analysis, Investigation, Validation. **Johannes Stiehm:** Formal analysis, Investigation, Validation. **Edwin C. Constable:** Supervision, Writing – review & editing. **Markus Lenz:** Funding acquisition, Project administration, Supervision, Writing – review & editing.

Declaration of Competing Interest

The authors declare that they have no known competing financial interests or personal relationships that could have appeared to influence the work reported in this paper.

Acknowledgements

This project has received funding from the European Union Horizon 2020 research and innovation programme under grant agreement No. 730105 (SCALE: www.scale-project.eu/). This work was supported by the Swiss State Secretariat for Education, Research and Innovation (SERI) under contract number 16.0155. We acknowledge the University of Basel for continuing support.

Appendix A. Supplementary data

Supplementary data to this article can be found online at https://doi.org/10.1016/j.hydromet.2022.105916.

References

Ahmad, Z., 2003. The properties and application of scandium-reinforced aluminum. JOM 55 (2), 35–39.
Almeida, M.I.G., Cattrall, R.W., Kolev, S.D., 2012. Recent trends in extraction and transport of metal ions using polymer inclusion membranes (PIMs). J. Membr. Sci. 415-416, 9–23.
Almeida, M.I.G.S., Cattrall, R.W., Kolev, S.D., 2017. Polymer inclusion membranes (PIMs) in chemical analysis - a review. Anal. Chim. Acta 987, 1–14.
Antony, J., 2014. Design of Experiments for Engineers and Scientists, 2 ed. Elsevier insights. Elsevier, Amsterdam. 221 pp.
Atkinson, A.C., Bogacka, B., Zhigljavski, A. (Eds.), 2001. Optimum design 2000; [Papers Presented Conference Optimum Design 2000: Prospects for the New Millennium, held in Cardiff, UK on April 12th - 14th, 2000]. Nonconvex Optimization and its Applications, 51. Kluwer Acad. Publ, Dordrecht, 306 pp.
Avdibegović, D., Zhang, W., Xu, J., Regadío, M., Koivula, R., Binnemans, K., 2019. Selective ion-exchange separation of scandium(III) over iron(III) by crystalline α-zirconium phosphate platelets under acidic conditions. Sep. Purif. Technol. 215, 81–90.
Bartkowska, M., Regel-Rosocka, M., Szymanowski, J., 2002. Extraction of zinc(II), iron (III) and iron(II) with binary mixtures containing tributyl phosphate and di(2-ethylhexyl)phosphoric acid or cyanex 302. Physicochem. Probl. Miner. Process. 36 (1), 217–224.
Batra, S., Awasthi, A., Iqbal, M., Datta, D., 2022. Solvent impregnated resins for the treatment of aqueous solutions containing different compounds: a review. Rev. Chem. Eng. 38 (2), 209–242.
Binnemans, K., Jones, P.T., Müller, T., Yurramendi, L., 2018. Rare earths and the balance problem: how to deal with changing markets? J. Sustain. Metall. 4 (1), 126–146.
Bordbar, H., Abedini, H., Yousefi, A.A., 2018. Parameters affecting reaction rate and conversion of TiO2 chlorination in a fluidized bed reactor: experimental and modeling approach. Trans. Nonferrous Metals Soc. China 28 (10), 2114–2124.
Cortina, J.L., Aguilar Sanjuán, M., 2008. Solvent Extraction and Liquid Membranes: Fundamentals and Applications in New Materials. Ion Exchange and Solvent Extraction. CRC Press, Boca Raton, 344 pp.
Croft, C.F., Almeida, M.I.G., Cattrall, R.W., Kolev, S.D., 2018. Separation of lanthanum (III), gadolinium(III) and ytterbium(III) from sulfuric acid solutions by using a polymer inclusion membrane. J. Membr. Sci. 545, 259–265.
Das, S., Behera, S.S., Murmu, B.M., Mohapatra, R.K., Mandal, D., Samantray, R., Parhi, P. K., Senanayake, G., 2018. Extraction of scandium(III) from acidic solutions using organo-phosphoric acid reagents: a comparative study. Sep. Purif. Technol. 202, 248–258.
Dean, A., Voss, D., Draguljić, D., 2017. Design and Analysis of Experiments, Second edition. Springer texts in statistics. Springer, New York. 840 pp.
Ditze, A., Kongolo, K., 1997. Recovery of scandium from magnesium, aluminium and iron scrap. Hydrometallurgy 44 (1–2), 179–184.
European Commission, 2017. On the 2017 List of Critical Raw Materials for the EU: COM (2017) 490 Final. Brussels, Belgium.
European Commission, 2020. Critical Raw Materials Resilience: Charting a Path towards Greater Security and Sustainability: COM/2020/474 Final. COM (2020) 474 Final. Brussels, Belgium.
Feuling, R.J., 1989. Recovery of Scandium, Yttrium and Lanthanides from Titanium Ore. US19890389088 C01F15/00;C01F17/00;C22B1/08;C22B1/10;C22B3/10;C22B3/16;C22B9/02;C22B34/12;C22B59/00;C01F17/00;C01G23/02.
Förstner, U., Salomons, W., Mader, P., 1995. Heavy Metals. Springer, Berlin Heidelberg, Berlin, Heidelberg.
Fröhlich, P., Lorenz, T., Martin, G., Brett, B., Bertau, M., 2017. Valuable metals-recovery processes, current trends, and recycling strategies. Angew. Chem. Int. Ed. Eng. 56 (10), 2544–2580.
Gajda, B., Bogacki, M.B., 2007. The effect of tributyl phosphate on the extraction of nickel(ii) and cobalt(ii) ions with di(2-ethylhexyl)phosphoric acid. Physicochem. Probl. Miner. Process. 41 (1), 145–152.
Gambogi, J., 2022. USGS Mineral Commodity Summary: Scandium.
Gao, L.-K., Rao, B., Dai, H.-X., Hong, Z., Xie, H.-Y., 2019. Separation and extraction of scandium and titanium from a refractory anatase lixivium by solvent extraction with D2EHPA and primary amine N1923. J. Chem. Eng. Japan/JCEJ 52 (11), 822–828.
Gázquez, M.J., Bolívar, J.P., Garcia-Tenorio, R., Vaca, F., 2014. A review of the production cycle of titanium dioxide pigment. MSA 05 (07), 441–458.
Hartley, C.J., Hazen, W.W., Baughman, D.R., Bemelmans, C.M.A., Belits, P.F., Lanyk, T. J., Porter, B.F., Liao, L., Mcallister, J., Yang, M.S.Y., 2014. Methods of Recovering Scandium from Titanium Residue Streams. US201414151177;US201361750867P C22B59/00.
Hedwig, S., Yagmurlu, B., Huang, D., von Arx, O., Dittrich, C., Constable, E.C., Friedrich, B., Lenz, M., 2022. Nanofiltration-enhanced solvent extraction of scandium from TiO 2 acid waste. ACS Sustain. Chem. Eng. 10 (18), 6063–6071.

Herring, J.S., 2012. Uranium uranium and thorium thorium resources uranium resources. In: Meyers, R.A. (Ed.), Encyclopedia of Sustainability Science and Technology. Springer, New York, New York, NY, pp. 11201–11219.
Hoffmann, M., Vaszita, E., Ujaczki, É., Fekete-Kertész, L., Molnár, M., Feigl, V., Adam, C., 2019. SCALE Deliverable D6.1 European Inventory of Scandium Containing by-Products. BAM, BME, NTUA, ITRB. https://ec.europa.eu/research/participants/documents/downloadPublic?documentIds=080166e5c7903051&appId=PPGMS.
Khorfan, S., Stas, J., Kassem, M., 1998. Stripping of uranium from Dehpa/kerosene solvents by different aqueous media. J. Radioanal. Nucl. Chem. 238 (1–2), 145–148.
Li, Y., Li, Q., Zhang, G., Zeng, L., Cao, Z., Guan, W., Wang, L., 2018. Separation and recovery of scandium and titanium from spent sulfuric acid solution from the titanium dioxide production process. Hydrometallurgy 178, 1–6.
Lide, D.R. (Ed.), 2004. CRC Handbook of Chemistry and Physics: A Ready-Reference Book of Chemical and Physical Data, 85. ed. CRC Press, Boca Raton, Getr. Zählung.
Nagul, E.A., Croft, C.F., Cattrall, R.W., Kolev, S.D., 2019. Nanostructural characterisation of polymer inclusion membranes using X-ray scattering. J. Membr. Sci. 588, 117208.
Nghiem, L., Mornane, P., Potter, I., Perera, J., Cattrall, R., Kolev, S., 2006. Extraction and transport of metal ions and small organic compounds using polymer inclusion membranes (PIMs). J. Membr. Sci. 281 (1–2), 7–41.
Ochsenkühn-Petropulu, M., Lyberopulu, T., Parissakis, G., 1995. Selective separation and determination of scandium from yttrium and lanthanides in red mud by a combined ion exchange/solvent extraction method. Anal. Chim. Acta 315 (1–2), 231–237.
Pei, L., Wang, L., Yu, G., 2011. Separation of Eu(III) with supported dispersion liquid membrane system containing D2EHPA as carrier and HNO3 solution as stripping solution. J. Rare Earths 29 (1), 7–14.
Perks, C., Mudd, G., 2019. Titanium, zirconium resources and production: a state of the art literature review. Ore Geol. Rev. 107, 629–646.
Reid, S., Tam, J., Yang, M., Azimi, G., 2017. Technospheric mining of rare earth elements from bauxite residue (red mud): process optimization, kinetic investigation, and microwave pretreatment. Sci. Rep. 7 (1), 15252.
Remmen, K., Schäfer, R., Hedwig, S., Wintgens, T., Wessling, M., Lenz, M., 2019. Layer-by-layer membrane modification allows scandium recovery by nanofiltration. Environ. Sci. Water Res. Technol. 5 (10), 1683–1688.
Shaltout, A.A., Seoudi, R., El-Ashkar, E.A., Eid, K.A., 2008. Developed method for spectroscopic studies of viscous samples. Anal. Lett. 41 (17), 3034–3048.
Shanghai Metals Market, 2022. Scandium Metal, USD/kg. https://www.metal.com/Rare-Earth-Metals/202104090004. Accessed 11 February 2022.
Sharaf, M., Yoshida, W., Kubota, F., Kolev, S.D., Goto, M., 2018. A polymer inclusion membrane composed of the binary carrier PC-88A and Versatic 10 for the selective separation and recovery of Sc. RSC Adv. 8 (16), 8631–8637.
Sholl, D.S., Lively, R.P., 2016. Seven chemical separations to change the world. Nature 532 (7600), 435–437.
Spivey, J.J., Berry, D.A., Shekhawat, D., 2011. Fuel Cells: Technologies for Fuel Processing, 1. Aufl. ed. Elsevier professional s.l., 568 pp.
Sugiura, M., Kikkawa, M., Urita, S., 1989. Carrier-mediated transport of rare earth ions through cellulose triacetate membranes. J. Membr. Sci. 42 (1–2), 47–55.
Sun, M., Liu, S., Zhang, Y., Liu, M., Yi, X., Hu, J., 2019. Insights into the saponification process of di(2-ethylhexyl) phosphoric acid extractant: thermodynamics and structural aspects. J. Mol. Liq. 280, 252–258.
Sykes, J.P., Wright, J.P., Trench, A., Miller, P., 2016. An assessment of the potential for transformational market growth amongst the critical metals. Appl. Earth Sci. 125 (1), 21–56.
U.S. Geological Survey, 2020. Mineral Commodity Summaries 2020. Mineral Commodity Summaries. Reston, VA, 204 pp. http://pubs.er.usgs.gov/publication/mcs2020.
Vahidi, E., Zhao, F., 2016. Life cycle analysis for solvent extraction of rare earth elements from aqueous solutions. In: Kirchain, R.E., Blanpain, B., Meskers, C., Olivetti, E., Apelian, D., Howarter, J., Kvithyld, A., Mishra, B., Neelameggham, N.R., Spangenberger, J. (Eds.), REWAS 2016. Springer International Publishing, Cham, pp. 113–120.
Vind, J., Malfliet, A., Bonomi, C., Paiste, P., Sajó, I.E., Blanpain, B., Tkaczyk, A.H., Vassiliadou, V., Panias, D., 2018. Modes of occurrences of scandium in Greek bauxite and bauxite residue. Miner. Eng. 123, 35–48.
Wang, W., Cheng, C.Y., 2011. Separation and purification of scandium by solvent extraction and related technologies: a review. J. Chem. Technol. Biotechnol. 86 (10), 1237–1246.
Wang, D., Li, Y., Wu, J., Xu, G., 1996. Mechanism of the extractant loss in lanthanide extraction process with saponified organophosphorus acid extraction systems - II: formation of aqueous aggregates: mechanism of the extractant loss in lanthanide extraction process with saponified organophosphorus acid extraction systems - II: formation of aqueous aggregates. Solv. Extract. Ion Exchang. 14 (4), 585–601.
Wang, W., Pranolo, Y., Cheng, C.Y., 2011. Metallurgical processes for scandium recovery from various resources: a review. Hydrometallurgy 108 (1–2), 100–108.
Wood, S.A., Samson, I.M., 2006. The aqueous geochemistry of gallium, germanium, indium and scandium. Ore Geol. Rev. 28 (1), 57–102.
Yagmurlu, B., Dittrich, C., Friedrich, B., 2017. Precipitation trends of scandium in synthetic red mud solutions with different precipitation agents. J. Sustain. Metall. 3 (1), 90–98.
Yoshida, W., Baba, Y., Kubota, F., Kolev, S.D., Goto, M., 2019a. Selective transport of scandium(III) across polymer inclusion membranes with improved stability which contain an amic acid carrier. J. Membr. Sci. 572, 291–299.
Yoshida, W., Kubota, F., Baba, Y., Kolev, S.D., Goto, M., 2019b. Separation and recovery of scandium from sulfate media by solvent extraction and polymer inclusion membranes with amic acid extractants. ACS Omega 4 (25), 21122–21130.